



Processing, Fabrication and Characterization of Advanced Target Sensors Using Mercury Cadmium Telluride (MCT)

**by F. Semendy, G. Brill, P. Wijewarnasuriya, Y. Chen, J. Sun, J. Bickford,
and N. Bambha**

ARL-TR-5292

September 2010

NOTICES

Disclaimers

The findings in this report are not to be construed as an official Department of the Army position unless so designated by other authorized documents.

Citation of manufacturer's or trade names does not constitute an official endorsement or approval of the use thereof.

Destroy this report when it is no longer needed. Do not return it to the originator.

Army Research Laboratory

Adelphi, MD 20783-1197

ARL-TR-5292

September 2010

Processing, Fabrication and Characterization of Advanced Target Sensors Using Mercury Cadmium Telluride (MCT)

**F. Semendy, G. Brill, P. Wijewarnasuriya, Y. Chen, J. Sun, J. Bickford,
and N. Bambha**

Sensors and Electron Devices Directorate, ARL

REPORT DOCUMENTATION PAGE

Form Approved
OMB No. 0704-0188

Public reporting burden for this collection of information is estimated to average 1 hour per response, including the time for reviewing instructions, searching existing data sources, gathering and maintaining the data needed, and completing and reviewing the collection information. Send comments regarding this burden estimate or any other aspect of this collection of information, including suggestions for reducing the burden, to Department of Defense, Washington Headquarters Services, Directorate for Information Operations and Reports (0704-0188), 1215 Jefferson Davis Highway, Suite 1204, Arlington, VA 22202-4302. Respondents should be aware that notwithstanding any other provision of law, no person shall be subject to any penalty for failing to comply with a collection of information if it does not display a currently valid OMB control number.

PLEASE DO NOT RETURN YOUR FORM TO THE ABOVE ADDRESS.

1. REPORT DATE (DD-MM-YYYY) September 2010		2. REPORT TYPE Final		3. DATES COVERED (From - To) 2009–2010	
4. TITLE AND SUBTITLE Processing, Fabrication and Characterization of Advanced Target Sensors Using Mercury Cadmium Telluride (MCT)				5a. CONTRACT NUMBER	
				5b. GRANT NUMBER	
				5c. PROGRAM ELEMENT NUMBER	
6. AUTHOR(S) F. Semendy, G. Brill, P. Wijewarnasuriya, Y. Chen, J. Sun, J. Bickford, and N. Bambha				5d. PROJECT NUMBER	
				5e. TASK NUMBER	
				5f. WORK UNIT NUMBER	
7. PERFORMING ORGANIZATION NAME(S) AND ADDRESS(ES) U.S. Army Research Laboratory ATTN: RDRL-SEE-I 2800 Powder Mill Road Adelphi, MD 20783-1197				8. PERFORMING ORGANIZATION REPORT NUMBER ARL-TR-5292	
9. SPONSORING/MONITORING AGENCY NAME(S) AND ADDRESS(ES)				10. SPONSOR/MONITOR'S ACRONYM(S)	
				11. SPONSOR/MONITOR'S REPORT NUMBER(S)	
12. DISTRIBUTION/AVAILABILITY STATEMENT Approved for public release; distribution unlimited.					
13. SUPPLEMENTARY NOTES					
14. ABSTRACT In this report the growth, processing, fabrication, and characterization of HgCdTe (or mercury cadmium telluride [MCT]) infrared (IR) detectors for advanced target detection are reported. The material was grown by solid source molecular beam epitaxy (MBE). Grown materials were characterized prior to processing to obtain information on carrier concentration, mobility and resistivity. Inductive coupled plasma (ICP) etching and metallization as required by the design of the sensors at different levels of processing were carried out using either AZ 5214 or AZ 9245 as photoresist masks. For the first time spin coating and lithography parameters were optimized with AZ9245 as the photoresist mask to achieve smooth surface and vertical side walls. An etch-through process of MCT and Si with a combined thickness of about 510 μm deep was carried out by ICP etching first by Ar/H ₂ gases followed by covering the sample by a thick AZ 9245 photoresist mask and Bosch process using SF ₆ , O ₂ and C ₄ F ₈ to detach the device from the base carrier silicon substrate. To understand the nature of the etching and to protect the surface of the detector, the wafers were periodically withdrawn and thickness of the photoresist measured. A twenty-step process finally yielded the desired ring type detectors that were used for electrical characterization and testing for target detection. The results of extensive steps involved in processing, device fabrication, material, and device characterizations are reported.					
15. SUBJECT TERMS MCT, processing, lithography, photodetector, sensors					
16. SECURITY CLASSIFICATION OF:			17. LIMITATION OF ABSTRACT UU	18. NUMBER OF PAGES 22	19a. NAME OF RESPONSIBLE PERSON Fred Semendy
a. REPORT Unclassified	b. ABSTRACT Unclassified	c. THIS PAGE Unclassified			19b. TELEPHONE NUMBER (Include area code) (301) 394-4627

Contents

List of Figures	iv
List of Tables	iv
1. Introduction	1
2. Experimental	2
3. Results and Discussion	9
4. Conclusions	12
5. References	13
List of Symbols, Abbreviations, and Acronyms	14
Distribution List	15

List of Figures

Figure 1. A slab of IR photodetector with a volume of l.w.d with the signal measured across the load resistor R_L	1
Figure 2. (a) Depiction of the ICP system, and (b) HgCdTe/CdTe/Si wafer on silicon carrier wafer thickness of the material and the surface of the devices.....	4
Figure 3. (a) HgCdTe/CdTe/Si wafer with PR, (b) after exposure and developing a pattern, and (c) after ICP dry etching of HgCdTe/CdTe/Si with Ar/H ₂ gas system.....	5
Figure 4. Two different PR thickness before and after etching the PR HgCdTe/CdTe/Si.....	6
Figure 5. Five different PR thickness measurements of PR before and in between, after etching the silicon substrate.....	7
Figure 6. (a) Etched HgCdTe/CdTe/Si wafer with PR, (b) DRIE ICP etching, and (c) after ICP-DRIE dry etched sample by BOSCH process.....	7
Figure 7. Percentage change in the thickness of the PR during and after the etch with respect to the original thickness of the PR.....	8
Figure 8. Nomarski microscope pictures of part of the fuze device, (a) fabricated device before etching, and (b) same part after etching.....	8
Figure 9. Nomarski microscope pictures of fabricated device, (a) before, and (b) after dry etching.....	9
Figure 10. Fabricated devices, (a) 1-in size fuze detector, (b) test detectors from a 3-in wafer, and (c) another fuze detector.....	9
Figure 11. Blackbody flood illumination measurement illustration.....	10
Figure 12. Example detector response versus bias plot (line illustrates linear variation in response to applied bias.....	11

List of Tables

Table 1. Representative blackbody test results for device comparison.....	11
---	----

1. Introduction

Infrared (IR) photodetectors are of great importance for military and civilian applications such as thermal imaging, heat seeking devices and proximity detection. IR detectors are divided into two categories: thermal and photon detectors (1, 2). Thermal detectors absorb incident radiation, increasing device temperature. This change in temperature, in turn, changes device resistance in the case of bolometric detectors and changes internal electric polarization in the case of pyroelectric detectors. Thermal detectors are inherently slow because the speed with which they change temperature is limited by their material's specific heat and density. Although they can operate at room temperature (RT), these detectors are typically thermoelectrically (TE) cooled for thermal stability (3, 4). In photon detectors, photon absorption causes generation of electron-hole pairs that give rise to an observable electrical signal. Photon detectors can be further divided into: (1) intrinsic direct band gap materials like HgCdTe (or mercury cadmium telluride [MCT]); (2) extrinsic type like Si (degenerately doped with In, Ga, Bi, As, P, or Sb) and Ge (doped with Au, Hg, Cd, Be, or Ga); or (3) photoemissive such as metal silicides and negative electron affinity materials. Photoconductive and photovoltaic phenomena are the two widely used modes for photo detection. Photon detectors are highly sensitive to radiation and operate only in a particular wavelength depending upon the bandgap of the material. The photoconductor, which is a sensor of choice in many applications, is designed in such a way that the electrons dominate the conductivity due to their high mobility, and holes play a secondary role. The operation of the photodiode is shown in figure 1. Photons of energy greater than the band gap energy E_g are absorbed to produce electron hole pairs. This in turn will change the electrical conductivity.

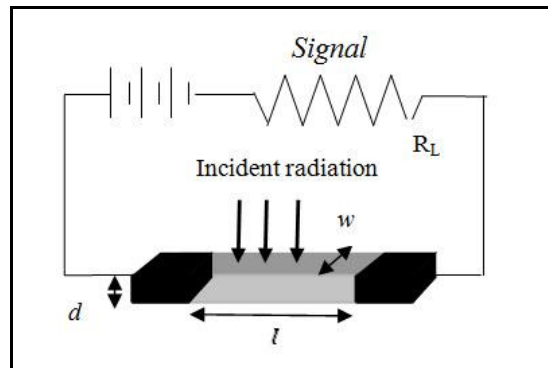


Figure 1. A slab of IR photodetector with a volume of $l.w.d$ with the signal measured across the load resistor R_L .

The change in conductivity is measured by means of electrodes attached to the detector. A bias voltage is applied to sense the change in the conductivity (5). The first results of photoconductivity in $Hg_{1-x}Cd_xTe$ were reported by Lawson et al. (6). A comparison of detector

performance using both one-dimensional and two-dimensional models have been reported (7, 8). For low resistance material, such as $\text{Hg}_{1-x}\text{Cd}_x\text{Te}$, the photoconductor is usually operated in a constant current circuit and the signal is detected as a charge in voltage developed across the load.

Infrared $\text{Hg}_{1-x}\text{Cd}_x\text{Te}$ MCT detectors can be designed properly to detect the presence of moving targets, or hot objects. These detectors can generally discriminate against various types of radiation. Such detection systems are generally known as fuze systems, which activates the mechanism in the vicinity of the target (9). In the past, passive systems have depended upon the hot exhaust of an aircraft, or exhaust of nozzles of aircraft and missiles, or molecular emission from hot gases. In many cases the fuzes can be prone to premature triggering on exhaust plumes. Such false triggering can be alleviated by proper design of the fuze. A high quality of design would include an optics and detector cells sensitive to radiation from the skin of the target due to kinetic heating, and insensitive to any other radiation. The fuze detector system can be designed in different shapes and forms. For example a circular type fuze has a central hole at the center for mounting and holding and with certain dimensions. Special attention must be paid to the opening in the $\text{Hg}_{1-x}\text{Cd}_x\text{Te}$ material and provisions must be made for attaching wires to the detector. A properly designed, processed, and fabricated $\text{Hg}_{1-x}\text{Cd}_x\text{Te}$ detector with proper optics will perform as a good proximity fuze and was the focus of this work.

2. Experimental

$\text{Hg}_{1-x}\text{Cd}_x\text{Te}$ material was grown by molecular beam epitaxy (MBE) using 3-in Si substrates. Although, a large lattice mismatch exists (19%), growth on Si substrates has the advantage of being able to fabricate numerous dies per wafer. This is especially advantageous when the device is large, as was the case for devices discussed in this report. To overcome the lattice mismatch issue, extensive research has gone into developing buffer layer technology that transitions from the Si lattice parameter to the HgCdTe lattice parameter while still maintaining high quality crystalline material. In summary, a thin ZnTe buffer layer is deposited by MBE and annealed followed by a thicker CdTe layer. During CdTe MBE growth, the growth is interrupted several times while the sample is annealed under an appropriate material flux. It has been determined recently that this annealing process is critical for obtaining high quality CdTe/Si material (10). Once growth is completed, the CdTe/Si material is known as a composite substrate. HgCdTe is then nucleated on this composite substrate using an MBE system capable of depositing Hg compounds. For the devices fabricated in this study, the HgCdTe layer thickness varied between 2 and 6 μm and had a cut-off wavelength varying between 2.5 and 5.0 μm measured at room temperature. All layers were characterized by Fourier Transform Infrared Spectroscopy (FTIR) prior to device fabrication. Additionally, some layers had representative pieces cleaved off from the larger 3-in sample for Hall measurements.

The lithographic processing of the $\text{Hg}_{1-x}\text{Cd}_x\text{Te}$ 3-in wafers must be carried out very carefully. There are a number of problems that arise when processing $\text{Hg}_{1-x}\text{Cd}_x\text{Te}/\text{Si}$. First, group II–VI materials are soft and highly sensitive to temperature. Second, after all the processing and metallization is completed, the sensor material ($\text{Hg}_{1-x}\text{Cd}_x\text{Te}$) and the substrate (silicon) must be dry etched away to separate the fabricated detector from the rest of the unprocessed material. Each of these steps raises special and unique problems and challenges due to the fact that the sensor material is soft and highly temperature sensitive. The lithographic process includes a number of baking at certain temperatures for a duration of time. This becomes a challenge with a thick photoresist (PR). A thick PR is required for the dry etching of the $\text{Hg}_{1-x}\text{Cd}_x\text{Te}/\text{Si}$. Since this type of deep etch is generally not performed for $\text{Hg}_{1-x}\text{Cd}_x\text{Te}/\text{Si}$ planar devices, new processes must be explored, tried and developed through experimentation. Second, dry inductive coupled plasma (ICP) etching needs to be done twice with a set of conditions to etch MCT and CdTe the buffer layer and another set of conditions to etch through the silicon substrate. The first etching is performed with a certain amount of argon and hydrogen gases at a pre-decided pressure, RF chuck power and ICP power to etch through the $\text{Hg}_{1-x}\text{Cd}_x\text{Te}/\text{CdTe}$ material. This etching is followed by a second ICP deep reactive ion etch (ICP-DRIE) also known as Bosch process using SF_6 , O_2 , and C_4F_8 . The Bosch process is composed of multiple steps of alteration between etching and deposition cycle. First, the silicon is etched in almost isotropic mode in short-time etch step with SF_6 gas and platen power. Then, a polymer layer, which serves to protect sidewall during the etching, is deposited on the silicon and mask with C_4F_8 gas. In the following step, the polymer layer is removed and the underneath silicon is subsequently etched away. There are several key process parameters in Bosch process, such as coil power platen power, gas flow rate, pressure, and duration time of etch/deposition process cycle. The platen power is employed to vary the substrate potential while the coil power is inductively coupled, which is the high power supply and is used to generate the plasma; the chamber pressure is normally controlled by varying the automatic pressure control valve and a high value indicates high pressure (11, 12). The controlling parameters can affect the resulting profile, the etch rate, and selectivity. The DRIE process affects the device's performance seriously; extreme measures must be taken to protect the surface by monitoring the surface by retrieving and measuring the photoresist thickness at least a number of times before the end point is reached. In plasma etching, micro-loading (13), which is present during etching and must be considered for the feature size of the elements the device under consideration. Micro-loading can be described as the interdependency between the etch rate and the aspect ratio. Usually the wider trenches etch faster than the narrow trenches. In the case of etch through, as in our case, it is necessary to consider an over etch time in order to compensate this difference of etch rate in wider and narrow trenches. Undesirable effects occur in the wide trenches over etched for a long time. But in our case this effect was minimal due to the optimized process we developed in our lab.

The HgCdTe wafers were cleaned in HF to remove the native oxide and used after further cleaning in acetone and isopropyl alcohol (IPA) and blow dried in acetone. It was spin coated with AZ 5214 and baked at $75\text{ }^\circ\text{C}$ for 30 min and exposed with appropriate mask for alignment

and mesa etch. The pattern was developed and surface cleaned for any hanging bonds by a descumming step using March RIE system. Wet etching technique was used to open up MCT as defined by the the mask using Br_2 in 100 ml lactic acid for about 60 s. The PR was removed using acetone and IPA and blow drying with N_2 . This was followed for in-situ CdTe contact hole lithography using standard procedures using AZ5214 PR. Holes were created by a wet etching technique using acid-dichromate solution. Test samples were cleaned in acid solution to remove native oxide and leaded in to an ebeam evaporator. Gold was deposited to a thickness of 3000 \AA at a pressure of 1×10^{-6} torr. The test sample was cleaned in acetone to remove all of the remaining PR. Next, as part of the design of the device, a passivation layer of CdTe was grown on top of the processed wafer. Using photolithography and AZ 5214, patterns were laid on top of the device and contact holes were opened up when exposed PR was developed, which was followed by another image by photo-lithography using the same PR. After proper preparation, Ti/Au in the amount of $200/3000 \text{ \AA}$ were deposited at a pressure of 1×10^{-6} torr in the e-beam evaporator. After proper cleaning of the wafer it was prepared again using standard photolithography using AZ 5214 PR with the soft bake done at $75 \text{ }^\circ\text{C}$ for 45 min and after exposure a hard bake at $90 \text{ }^\circ\text{C}$ for 3 min. After developing the pattern for support metal, the wafer was descummed and acid dipped prior to loading on to the e-beam evaporator. At a pressure of 1×10^{-6} torr support metals Ti/Au ($300, 9000 \text{ \AA}$) were deposited with careful deposition of Au in three steps with a waiting time of 45 min in between to avoid any over heating of detector material. Once the metallization was complete, samples were retrieved and PR removed using the conventional techniques and inspected. Processed wafers, which appeared without any imperfections with the fuze detector pattern, were chosen for further steps of fabrication. Figure 2 shows (a) the etch ICP etch system and (b) the etching material HgCdTe/CdTe/Si mounted on a carrier Si wafer. In figure 2 (b) the rings indicate the surface depiction of the plasma of the device and the red circles indicate position of the thickness measurement of the PR before and after etching.

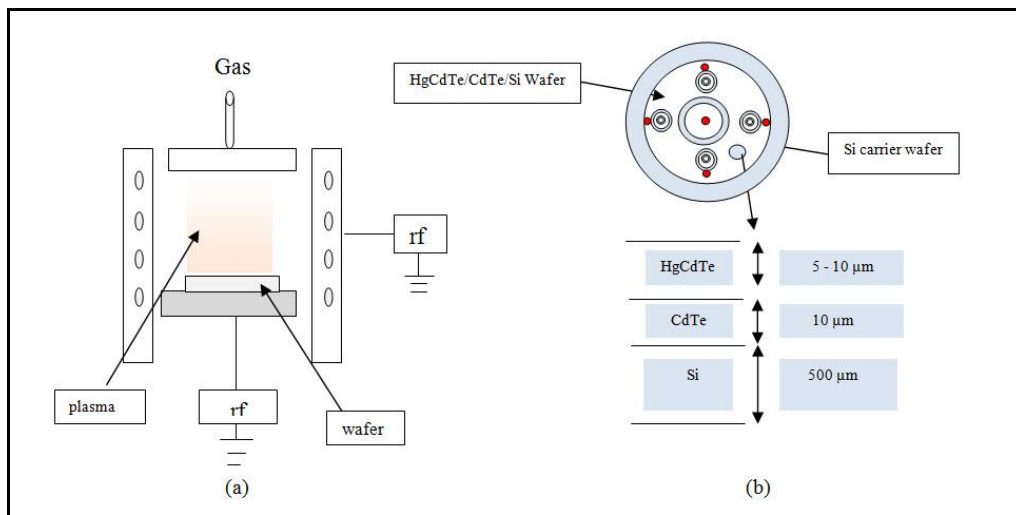


Figure 2. (a) Depiction of the ICP system, and (b) HgCdTe/CdTe/Si wafer on silicon carrier wafer thickness of the material and the surface of the devices.

The next important step in fabricating the device is to vertically dry etch MCT/CdTe/Si as part of the etch through and separate the device from the mother wafer. Since the entire thickness of the MCT film had to be removed, standard PR such as AZ5214 cannot be used because of the selectivity issues. There will be substantial erosion of the resist due to the damage that can be caused by the etching gases. Hence we substitute AZ 9245 as the PR of choice. It is a thick PR and will provide high resolution, superior aspect ratio and wide focus, exposure latitude, and good sidewall profiles. Patterns can be developed in inorganic based potassium hydroxide. However, AZ 9245 has never been used with MCT for a large scale and almost 3-h dry etch processing. Hence we found it a challenge to optimize the etch steps and procedures for II–VI MCT. In our newly developed proprietary process, a typical processing of the MCT etching includes spinning AZ 9245 at 1000 rpm and baking at 80 °C for 60 min followed by leaving the wafer at room temperature for 60 min to absorb the moisture. The wafer was aligned and photo-exposed using a Karl Susse MA-6; the wafer was developed in AZ 400 K developer, which was followed by baking the sample at 90 °C for 15 min on a hot plate. The sample was left at RT for another 2 h before processing. The 3-in wafer was then mounted on a 4-in carrier Si wafer using cool grease. For it to stick to the 4-in wafer surface it was heated at 50 °C for 1 min. Oxford Plasmalab system 100 ICP-RIE system was used to etch the MCT wafer. It has a 13.56 MHz driven parallel plate reactor. To etch the wafer we used Ar/H₂ (45 sccm/45 sccm) gas system with 10 mT pressure, ICP power of 800 W, and RF power of 50 W. Care was taken to measure the five point (as depicted in figure 2 (b) by the red circle) thickness of the PR before and after etch. The material etching is with the PR mask and is indicated in figure 3.

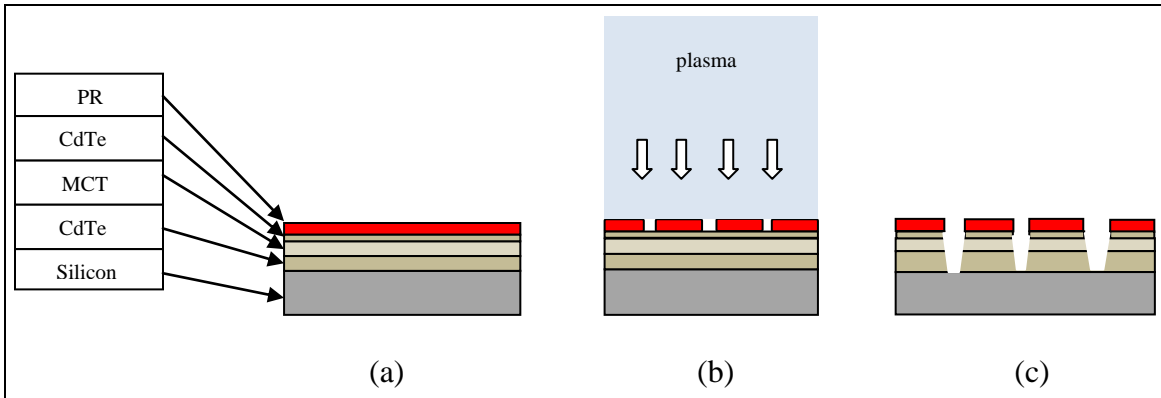


Figure 3. (a) HgCdTe/CdTe/Si wafer with PR, (b) after exposure and developing a pattern, and (c) after ICP dry etching of HgCdTe/CdTe/Si with Ar/H₂ gas system.

An additional step of measuring the thickness midway during etching was also included as part of the monitoring of PR thickness after etch stop and retrieving the sample. The measured thickness of PR is shown in figure 4.

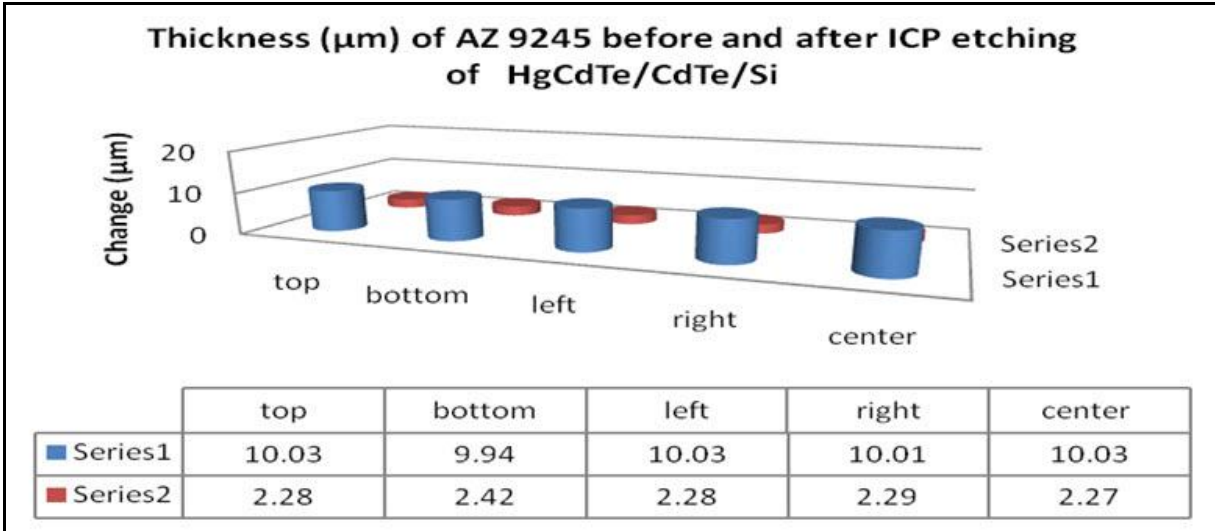


Figure 4. Two different PR thickness before and after etching the PR HgCdTe/CdTe/Si.

The blue cylindrical illustrations indicate the thickness measurements of PR before etching and the red are after etching. Calculations indicate a markedly reduced thickness of the PR of about 80% between the two states. The MCT 3-in wafer was detached from the carrier 4-in silicon wafer and cleaned thoroughly with acetone and IPA and removed of all PR with a final stop of RIE O_2 descumming etch for 90 s to remove the PR at low RF power. The optical patterning was repeated with the AZ 9245 deposited at 1000 rpm for 40 s. The wafer was soft baked at 80°C for 60 min followed by exposure with the mask. The pattern was developed using AZ 400 K developer and cleaned carefully using deionized water and blow dried using nitrogen. The wafer was then baked at 90°C for 15 min on a hot plate and left at room temperature for 60 min. The wafer was mounted a 4-in silicon wafer for ICP-DRIE etch through to separate the fuze detectors. As part of the plan to make sure that there is enough PR to protect the MCT surface, the wafer was periodically withdrawn and thickness of the PR was carried out about five times. The etch rate for the silicon using Bosch process is about $3\ \mu\text{m}/\text{min}$, which will give a calculated time to etch a $500\text{-}\mu\text{m}$ silicon wafer about 2.8 h (~ 10000 s). The measurement of the thickness of PR at five different positions as indicated in figure 2 (b) at five different times are recorded and the graphical representation is shown in figure 5.

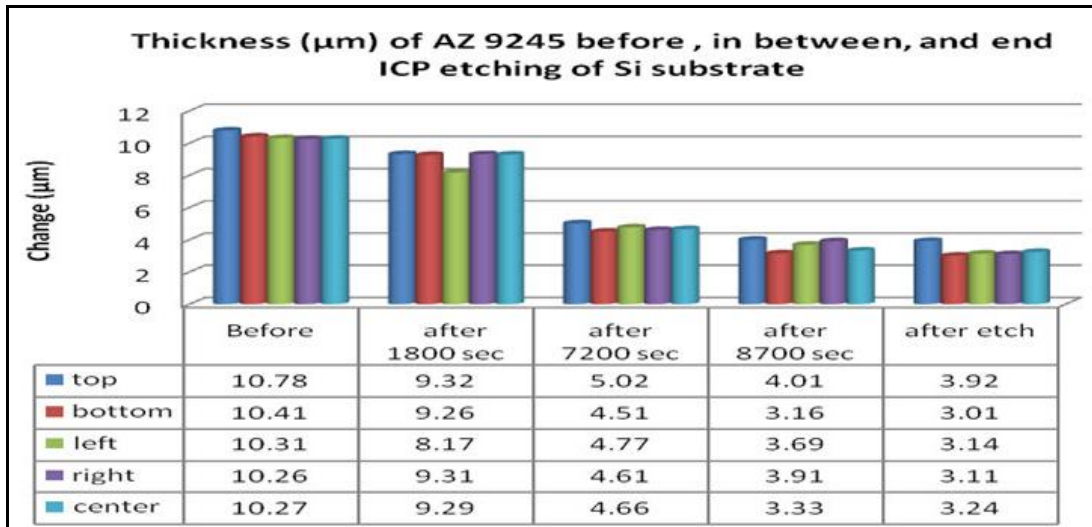


Figure 5. Five different PR thickness measurements of PR before and in between, after etching the silicon substrate.

In figure 6 the ICP-DRIE etch using Bosch process is depicted. The full etch through of the silicon wafer took about 10000 s for completion.

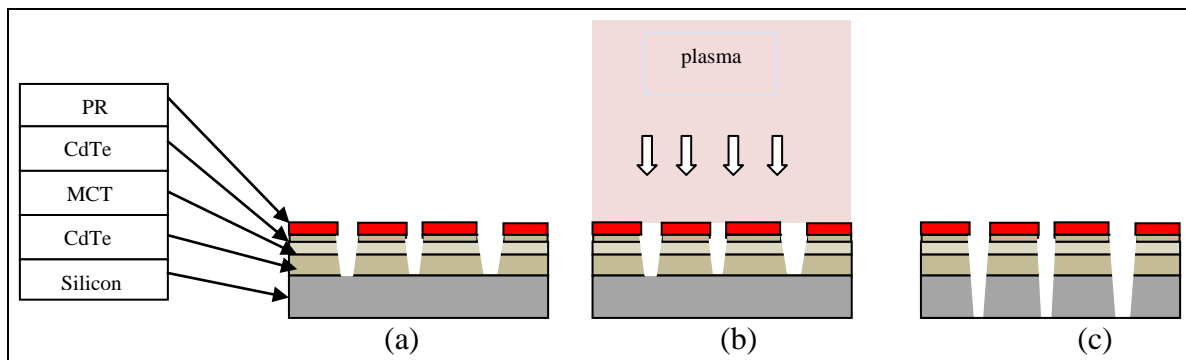


Figure 6. (a) Etched HdCdTe/CdTe/Si wafer with PR, (b) DRIE ICP etching, and (c) after ICP-DRIE dry etched sample by BOSCH process.

Figure 7 illustrates the percentage change in the thickness of the PR during and after the etch with respect to the original thickness. One can observe that a drastic reduction in the thickness occurs between the second and third measurements. The larger difference is due to the time difference in measurements. However, after the next measurement the thickness difference does not show a major change. This may possibly be due to back filling and saturation.

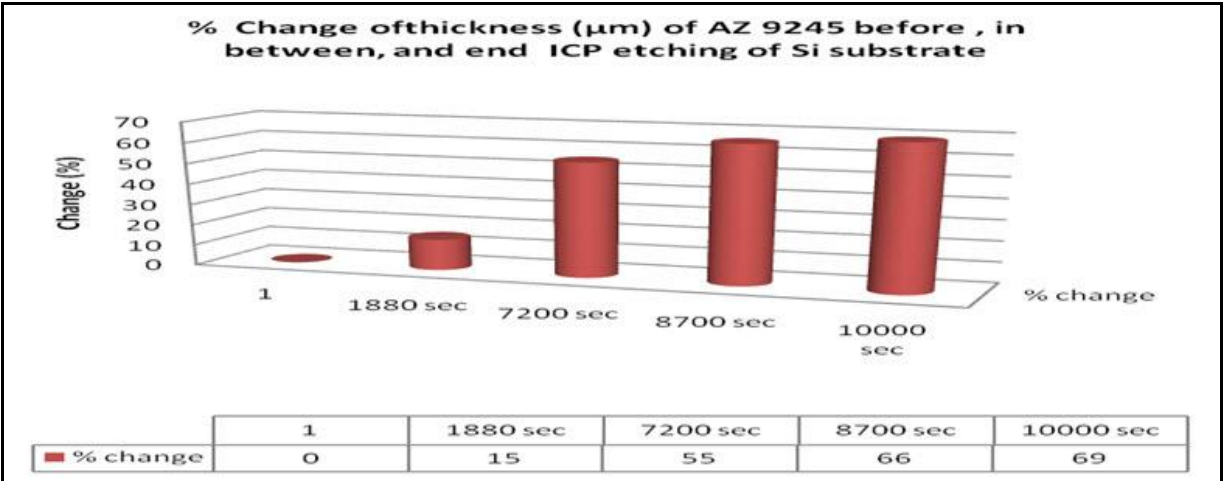


Figure 7. Percentage change in the thickness of the PR during and after the etch with respect to the original thickness of the PR.

In our fabrication of devices and subsequent steps, we were extremely careful in pursuing the step-by-step processing of lithography and dry etching. This extreme care was necessary and has produced quality undamaged surface as can be observed in the surfaces of the fabricated devices, as seen by the microscopic pictures in figures 8 (a), (b) and 9 (a), (b). This certainly indicates that the process developed in the U.S. Army Research Laboratory (ARL) is a desirable procedure in protecting the surface of the MCT while processing and dry etching test samples for an extended period of time. This newly developed procedure enabled us to fabricate MCT/CdTe/Si based thick photo detectors.

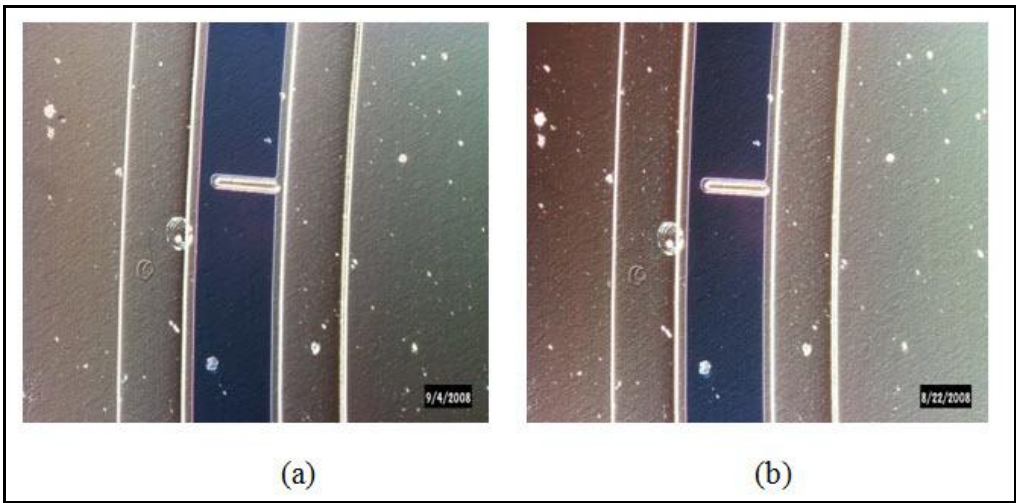


Figure 8. Nomarski microscope pictures of part of the fuze device, (a) fabricated device before etching, and (b) same part after etching.

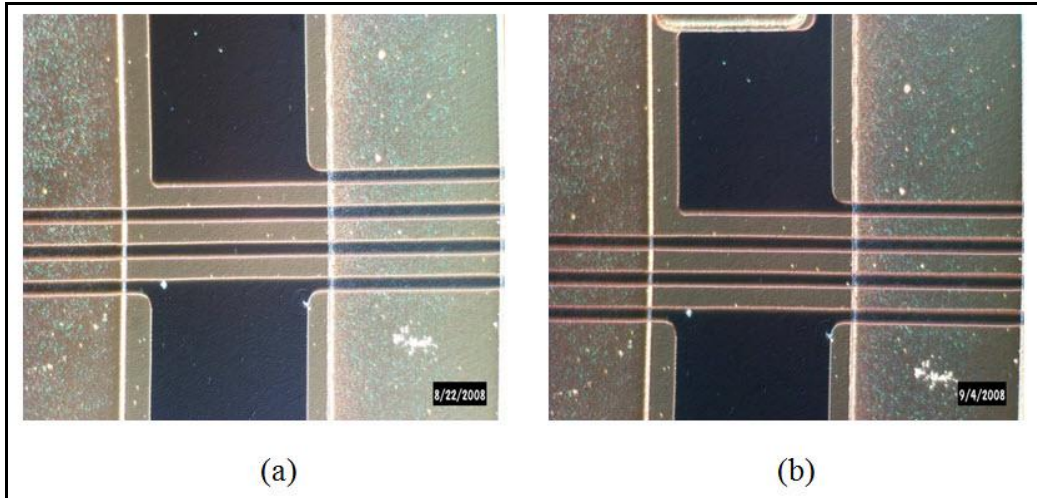


Figure 9. Nomarski microscope pictures of fabricated device, (a) before, and (b) after dry etching.

3. Results and Discussion

The pictures of the fabricated fuze devices are given below in figure 10. Figure 10 (a), (b), and (c) show detectors fabricated from a single 3-in wafer using the ARL developed procedure. Yellow rings indicate metal and grey colored parts indicate the sensing material.

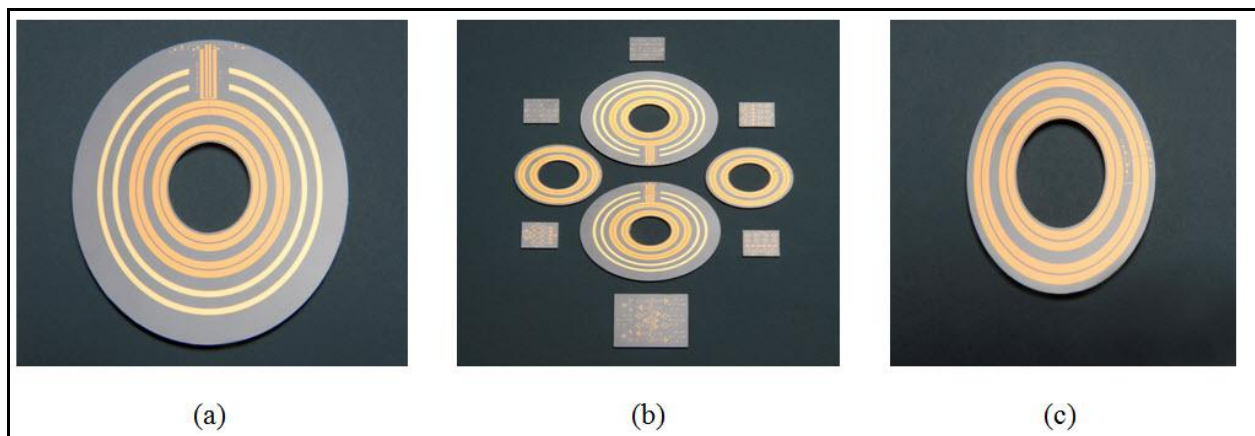


Figure 10. Fabricated devices, (a) 1-in size fuze detector, (b) test detectors from a 3-in wafer, and (c) another fuze detector.

The fuze devices have detector active areas, bond pads, and openings at the center to accommodate lens system. In a final assembly, the detector fuze and the wires will be encapsulated to protect them from damages.

Test devices consisted of both square and tactical ring geometries. Several different devices were tested and compared across various growth and fabrication iterations to understand their

impact. Measurements were taken using a calibrated blackbody source at a specific temperature T , set a given distance away from the detectors d , and apertured with a circular opening of diameter D as shown in figure 11. Given that the blackbody source used has a nearly spectrally flat emissivity ε of 0.99, the full-spectrum Incidence E in W/m^2 shining on the detector is given by equation 1, where σ is Stefan-Boltzmann's constant equal to approximately $5.67\text{e-}8 \text{ W}/(\text{m}^2\cdot\text{K}^4)$. This full-spectrum Incidence is used to characterize the detectors because the relative spectral response of each detector was not accounted for.

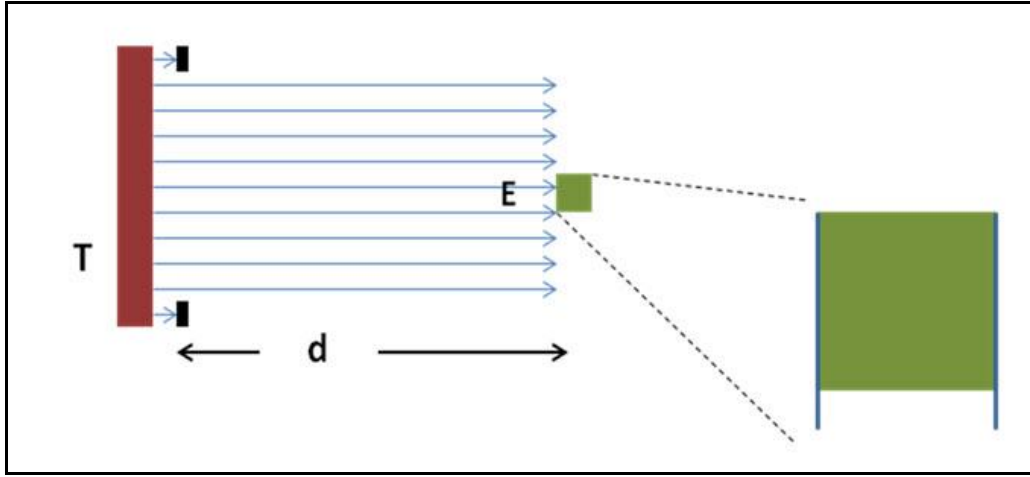


Figure 11. Blackbody flood illumination measurement illustration.

$$\text{Incidence} \equiv E = \varepsilon \sigma (T_{\text{Blackbody}}^4 - T_{\text{Ambient}}^4) \cdot \left(\frac{(D/2)^2}{d^2 + (D/2)^2} \right) \quad (1)$$

Photoconductors exhibit a change in resistance that is linearly proportional to their incident power, which is the product of incidence E and device area A . This linear response continues from negligible incident power up to the detector's saturation limit. This limit was not exceeded during testing and all data presented here is from within the linear incident power region. Each photoconductor's change in resistance is easily compared with other similar sized and shaped devices if the incident power is accounted for as shown in equation 2 (represented in W^{-1}).

$$\frac{R_{\text{light}} - R_{\text{dark}}}{R_{\text{dark}}} \left(\frac{1}{E \cdot A} \right) = \frac{\Delta R}{R_{\text{dark}}} \left(\frac{1}{E \cdot A} \right) \quad (2)$$

The change in resistance is divided by the device's dark resistance in order to normalize each device's change in resistance versus bias. This ratio is used because any given device's change in resistance is linearly proportional to its bias voltage up to its saturation bias. By staying below this saturation level the slope of this linear proportion can be described by this ratio of change of resistance over dark resistance as shown in figure 12.

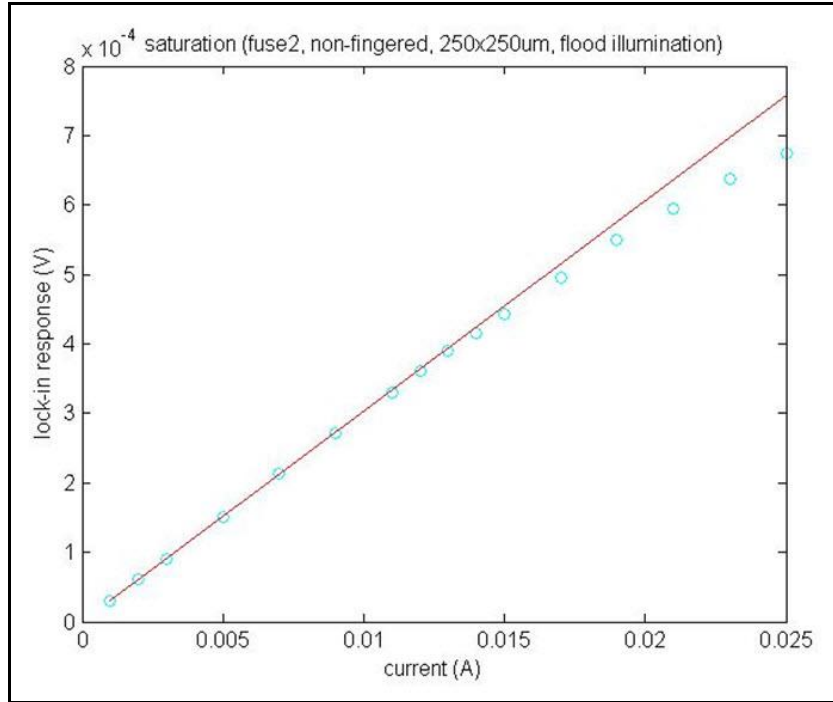


Figure 12. Example detector response versus bias plot (line illustrates linear variation in response to applied bias).

This figure of merit is invariant for a given device geometry and size and varies only with device material and contact characteristics. In this way duplicate device geometries and sizes in separate runs can be used to compare growth and fabrication variations consistently. Deriving a device geometry and size invariant figure of merit is therefore beyond the scope of this study. Select device results are shown in table 1.

Table 1. Representative blackbody test results for device comparison.

Device	$R_{\text{dark}} (\Omega)$	Area (m^2)	Incidence (W/m^2)	Response (W^{-1})
HgCdTe fuze #2 250 μm ×250 μm	101.0	6.25E-8	35.541	1.332E+3
HgCdTe fuze #5 250 μm ×250 μm	327.96	6.25E-8	2.897	5.811E+3
HgCdTe fuze #7 250 μm ×250 μm	197.61	6.25E-8	2.897	2.168E+3
HgCdTe fuze #11 250 μm ×250 μm	78.28	6.25E-8	2.897	2.661E+2
HgCdTe fuze #14 250 μm ×250 μm	4864	6.25E-8	2.897	–
HgCdTe fuze #15 250 μm ×250 μm	10058	6.25E-8	2.897	–
HgCdTe fuze #19 250 μm ×250 μm	contacts nonlinear	–	–	–

Although the data shows considerable measurement variance, table 1 shows an improvement in response figure of merit with higher dark resistance. This was the motivation to purposefully increase the HgCdTe resistivity. The resistance was improved by increasing the Cd composition, which yielded a higher bandgap. This higher bandgap increased the resistance by having less free carriers at room temperature. In addition to increasing the resistance, the higher bandgap also decreased the absorption cutoff wavelength causing the responsivity to decrease. In addition, the higher bandgap also made electrical contact to the devices much more resistive. The highest Cd composition devices tested (fuze #19) had nonlinear contacts, whose measurement results could not be fairly compared. Some batches of HgCdTe suffered from unintentional doping, as well, which lowered device resistance. In future revisions the Cd composition should be optimized, along with contact resistivity, and the unintentional doping lowered as much as possible to create the best possible device candidate material.

4. Conclusions

We reported the growth, processing, fabrication and characterization of HgCdTe IR detectors for advanced target detection. The material was grown by solid source MBE. Grown materials were characterized prior to processing to obtain information on carrier concentration, mobility and resistivity. ICP etching and metallization as required by the design of the sensors at different levels were carried out using either AZ 5214 or AZ 9245 as PR masks. For the first time spin coating and lithography parameters were optimized with AZ9245 as the PR mask to achieve smooth surface and vertical side walls. An etch-through process of MCT and Si with a combined thickness of about 510- μm deep was carried out by ICP etching first by Ar/H₂ gases followed by a deposition and photolithography with AZ 9245 PR mask, and a DRIE using SF₆, O₂, and C₄F₈ gas chemistry by the Bosch etch process to detach the device from the base carrier silicon substrate. To understand the nature of the etching and to protect the surface of the detector, the wafers were periodically withdrawn and thickness of the PR measured. A twenty-step process finally yielded the desired ring type as well as other test detectors that were used for electrical characterization and testing for target detection. The data shows considerable measurement variance, an improvement in response figure of merit with higher dark resistance. This was the motivation to purposefully increase the HgCdTe resistivity. The resistance was made to improve by increasing the Cd composition, which yielded a higher bandgap. This higher bandgap increased the resistance by having less free carriers at RT. In addition to increasing the resistance, the higher bandgap also decreased the absorption cutoff wavelength causing the responsivity to decrease. In addition, the higher bandgap also made electrical contact to the devices much more resistive. The highest Cd composition devices tested had nonlinear contacts, whose measurement results could not be fairly compared. Some batches of HgCdTe suffered from unintentional doping as well, which lowered device resistance. In future revisions the Cd composition should be optimized, along with contact resistivity, and the unintentional doping lowered as much as possible to create the best possible device candidate material.

5. References

1. Longand, D.; Schmit, J. L. Mercury-cadmium Telluride and Closely Related Alloys. In *Semiconductors and Semimetals*; Willardson, R. K., Beer, A. C. Eds.; Vol 5, Academic Press: New York, 1970, pp 175–255.
2. Michael, E.; Razeghi, M. *Opto-electronics rev* **1998**, 6 (1), 11–23.
3. Rogalskiand, A.; Piotrowski, J. *J. Intrinsic Infrared detectors, Prog. Quant. Electr.* **1988**, 12, 87–289.
4. Singh, R.; Mittal, V. *Defense Sci. Jnl* **2003**, 53 (3), 281–324.
5. Ritter, E. S. Electron Process in Photodetectors. In *Photoconductivity Conference*; Backeridge, R., Russel, B., Hahn, E., Eds.; Atlantic City, 1954, Wiley: New York, 1956, pp 215–66.
6. Lawson, W. D.; Neilson, S.; Putley, E. H.; Young, A. S. Preparation and Properties of HgTe and Mixed Crystals of HgTe-CdTe. *J. Phys. Chem. Solids.* **1959**, 9, 325–329.
7. Kolodny; Kidron, I. Two Dimensional Effects in Intrinsic Photoconductive Detectors. *Infrared Physics* **1982**, 22, 9–22.
8. Smith, E.P.G; Musca, C. A.; Farone, L. Two Dimensional Modeling of HgCdTe Photoconductive Detectors. *Infrared Phys. and Technol.* **2000**, 41, 175–186.
9. [Http://www.fas.org/man/dod-101/navy/docs/fun/part14.htm](http://www.fas.org/man/dod-101/navy/docs/fun/part14.htm) (Accessed 07/26/2010).
10. Chen, Y.; Farrell, S.; Brill, G.; Wijewarnasuriya, P.; Dhar, N. *J. Crystal Growth* **2008**, 310 (24), 5303–5307.
11. McAuley, S. A.; Ashraf, H.; Atabo, L.; Chambers, A.; Hall, S.; Hopkins, J.; Nicholls, G. **2001**, 34, 2769–2774.
12. Pendharkar, S. V.; Wolfe, J. C.; Ramprasad, H. R.; Chau, Y. L.; Licon, D. L.; Morgan, M. D.; Horne, W. E.; Tiberio, R. C.; Randall, J. N. *Jnl. Vac. Sci. & Tech, B* **1995**, 13, 2588–2592.
13. Kuhl, K.; Vogel; Schaber, U.; Scafflik, R.; Hillerich, B. *SPIE* **1998**, 3511, 97–105.

List of Symbols, Abbreviations, and Acronyms

ARL	U.S. Army Research Laboratory
FTIR	Fourier Transform Infrared Spectroscopy
ICP	inductive coupled plasma
ICP-DRIE	ICP deep reactive ion etch
IPA	isopropyl alcohol
IR	infrared
MBE	molecular beam epitaxy
MCT	mercury cadmium telluride
PR	photoresist
RT	room temperature
TE	thermoelectrically

NO. OF
COPIES ORGANIZATION

1 ADMNSTR
ELEC DEFNS TECHL INFO CTR
ATTN DTIC OCP
8725 JOHN J KINGMAN RD STE 0944
FT BELVOIR VA 22060-6218

1 CD OFC OF THE SECY OF DEFNS
ATTN ODDRE (R&AT)
THE PENTAGON
WASHINGTON DC 20301-3080

1 US ARMY RSRCH DEV AND ENGRG
CMND
ARMAMENT RSRCH DEV & ENGRG
CTR
ARMAMENT ENGRG & TECHNLOGY
CTR
ATTN AMSRD AAR AEF T J MATTS
BLDG 305
ABERDEEN PROVING GROUND MD
21005-5001

1 PM TIMS PROFILER (MMS P)
AN/TMQ-52
ATTN B GRIFFIES
BUILDING 563
FT MONMOUTH NJ 07703

1 US ARMY INFO SYS ENGRG CMND
ATTN AMSEL IE TD A RIVERA
FT HUACHUCA AZ 85613-5300

1 COMMANDER
US ARMY RDECOM
ATTN AMSRD AMR
W C MCCORKLE
5400 FOWLER RD
REDSTONE ARSENAL AL
35898-5000

1 US GOVERNMENT PRINT OFF
DEPOSITORY RECEIVING SECTION
ATTN MAIL STOP IDAD J TATE
732 NORTH CAPITOL ST NW
WASHINGTON DC 20402

1 US ARMY RSRCH LAB
ATTN RDRL CIM G T LANDFRIED
BLDG 4600
ABERDEEN PROVING GROUND MD
21005-5066

NO. OF
COPIES ORGANIZATION

9 US ARMY RSRCH LAB
ATTN IMNE ALC HRR
MAIL & RECORDS MGMT
ATTN RDRL CIM L TECHL LIB
ATTN RDRL CIM P TECHL PUB
ATTN RDRL SEE I G BRILL
ATTN RDRL SEE I F SEMENDY
ATTN RDRL SEE I
P WIJEWARNASURIYA
ATTN RDRL SEE I J SUN
ATTN RDRL SEE M J BICKFORD
ATTN RDRL SEE M N BAMBHA
ADELPHI MD 20783-1197

INTENTIONALLY LEFT BLANK.